Experimental Investigation of Pin Fin Heat Sink Effectiveness

Massimiliano Rizzi,
Marco Canino, Kunzhong Hu,
Stanley Jones, Vladimir Travkin, Ivan Catton
MAE Department, 48-121 Engineering IV, UCLA
Los Angeles, CA 90024-1597

Abstract
This paper will describe an experimental investigation of heat sink effectiveness. The heat sinks were constructed of aluminum and consisted of an array of staggered pin fins. Each of the three heat sinks had constant fin height, constant fin diameter, but the pitch was varied. The three interstitial (distance from pin center to pin center measured diagonally) pitches used were: P/d = 3/1, 9/4, 3/2. Heat generation was accomplished using cartridge heaters inserted into a copper block.. The high thermal conductivity of the copper ensured that the surface beneath the heat sink would be constant temperature.
A constant surface temperature was desired because the application was a heat sink which removes heat from a IGBT microchip. An array of 16 different type T thermocouples were arranged on the surface of the heat sink. Eight of the thermocouples measured air temperature at several locations in the heat sink while the other eight measured surface temperatures. On three of the fins the temperature distribution of the fin was measured (fin base temperature, mid-fin temperature, and fin tip temperature).
The cooling fluid was air and the experiments were conducted with a Reynolds number based on a porous media type hydraulic diameter ranging from 400 to 17000. The channel had a shroud that touches the fin tips, eliminating any flow bypass. The experimental results were compared to a numerical algorithm based on VAT (volume averaged theory) calculations. A number of data reduction parameters and procedures were developed using scaling heterogeneous formulation by VAT. A correlation relating heat transfer performance to Reynolds number and other important characteristic parameters is given and the results are compared to the literature.

Nomenclature

d_{por}	Characteristic length [m]
$E_{eff}1$	Effectiveness of heat transfer per unit volume [1/K]
f_f	Momentum resistance in the volume [-]
k_c	Conductivity coolant coefficient [W/m K]
h_r	Global heat transfer coefficient of the reference flat bottom plate with the same hydraulic resistance ς
H_r	Heat transfer rate per unit volume per unit temperature difference [W/m^{3}K]
L_x	Length of the heat sink [m]
$\langle m \rangle$	Porosity [-]
Nu_w	Bottom wall Nusselt number [-]
P_p	Pumping power per unit of volume [W/m^3]
q_w	Heat flux through the bottom surface of the heat sink [W/m^2]
S_{all}	Internal surface [m^2]
S_w^*	The overall specific surface per unit volume of heat exchange [1/m]
$S_{w\text{int}}$	Internal wetted surface [m^2]
S_{wb}	Bottom wetted surface [m^2]
$T_a(x)$	Averaged temperature over vertical coordinate (y) mass flow [K]
T_{bc}	Bulk temperature of the coolant [K]
α_w^*	Combined (averaged over the all internal surfaces) heat transfer coefficient [W/m^{2}K]
$T_{\max}$	Maximum temperature of the wall [K]
$\tilde{\tilde{U}}_b$	Averaged interstitial bulk velocity [m/s]
ς	Normalized hydraulic resistance
Ω	Volume of the heat sink [m^3]
ρ_f	Density of the coolant fluid [kg/m^3]

I. INTRODUCTION

The primary goal in semiconductor heat sink design is simple. It is to increase the heat transfer while decreasing the momentum resistance as for regular closed type heat exchangers is the goal. Nevertheless, as soon as everyone agrees that the best way to achieve the maximum heat transfer rate within a particular volume of heat sink is through the introduction of additional heat exchanging elements (ribs or pins of different shape) the problem becomes a two scale heterogeneous volumetric heat exchanger design problem. The processes on the lower scale heat transport – in and around a single transfer element (rib, fin) no longer describe the heat transfer rate of the whole sink. At the same time, the formulation of the problem of a heat sink for a one-temperature, or even a two-temperature homogeneous medium does not involve or connect the local (lower scale) transport characteristics determined by the morphology of the surface elements, directly to the performance of heat sink nor does it give guidance on how to improve the performance characteristics.

In our effort to tie the experimental characteristics of heat sink to the theoretical scaled (VAT) description and simulation of semiconductor base-to-air heat sinks, we came

to the process of coupling of two scale modeling and experiment for heat sink design. Most past work focused on the upper scale performance characteristics resulting in many efforts to measure the bulk heat transport rate and in modeling of numerous morphologies (see, for example, Andrews and Fletcher (1996), Bejan and Morega, (1993); Bejan, (1995); Fabbri (1999); Jubran, Hamdan, and Abdualh (1993); Kim and Kim (1999); You and Chang (1997), etc.). In many cases, the experimental was data reduced to the homogeneous device effectiveness:

$$E_{eff3} = \frac{Nu}{f_f^{1/3}\,Re}$$

where f_f is the momentum resistance in the volume, and Re is be constructed using only one geometric parameter. The two scale, VAT upper scale governing equations applicable to this problem, contain four additional descriptive terms in the momentum equation (for 1D turbulent equation), seven terms in the fluid temperature equation, and five additional terms in the solid phase (reflecting heat transport through ribs, pins) temperature equations (Gratton et al. 1996; Travkin et al., 2000).

At the present time, little known about experimental needed for development of experimental closure or verification of VAT heat exchanger governing equations. Contrary to simulation numerical experiments, the physical experiment is usually much more restrictive in terms of the number of local experimental points that can be obtained. It is a problem to properly make local measurements and to relate the measurements within the volume of the heat exchange device to the results from simulations because the data point is a pint value and the simulation value is an average over a volume of finite size. In this experiment we attempt to deal with both. We analyze effectiveness models by Andrews and Fletcher (1996), You and Chang (1997), Fabbri (1999), among others, in effort to reveal the positive features in them. Andrews, M.J. and Fletcher, L.S. (1996), provide comparisons of a wide variety of heat enhancing technologies based on the parameter of heat transfer rate per unit volume per unit temperature difference ($S_{all}\overline{\alpha}_{all}/\Omega$) and pumping power per unit volume $\frac{P}{\Omega}\left[\frac{W}{m^3}\right] = \frac{\dot{m}\Delta P}{\rho_f\,\Omega}$.

You and Chang (1997) calculated the local Nusselt number for the flat channel with rectangular pin fins via:

$$Nu_x(x) = \frac{h_w(x)D^*}{k_f} = \frac{D^*}{k_f(T_w(x)-T_a(x))}\times\left(-\langle m\rangle^2 k_f\left(\frac{\partial T_f}{\partial y}\right)_w - \langle 1-m\rangle^2 k_s\left(\frac{\partial T_s}{\partial y}\right)_w\right)$$

$$D^* = d_{por} = \frac{4\langle m\rangle}{S_w},$$

$$h_w = \frac{q''(x)}{(T_w(x)-T_a(x))} = \frac{\left(-\langle m\rangle^2 k_f\left(\frac{\partial T_f}{\partial y}\right)_w - \langle 1-m\rangle^2 k_s\left(\frac{\partial T_s}{\partial y}\right)_w\right)}{(T_w(x)-T_a(x))},$$

where $T_a(x)$ is the velocity weighted cross-stream average air temperature:

$$T_a(x) = \frac{1}{\delta U}\int_0^{\delta} T_f(y)u(y)\,dy.$$

The average Nu over the length of the sample is

$$Nu = \frac{1}{L}\int_0^L Nu_x(x)\,dx,\ \mathrm{Re} = \langle m\rangle \mathrm{Re}_{por} = \frac{\tilde{U}\,4\langle m\rangle^2}{\nu\,S_w}.$$

This Nusselt number is not an internal surface Nu_{in}, because the is flux determined by heat transport in both phases.

Among the results You and Chang (1997) obtained there is a note on p. 842 that indicates that: "It should be noted that the Nusselt number is not dependent on the applied wall heat flux." Fabbri (1999) calculated for the laminar regime Nu_e (equivalent) number in the flat channel with longitudinal rib fins using the following:

$$h = \frac{q''}{(T_{\max} - T_{bc})}, \quad Nu_e = \frac{h(2H)}{k_c},$$

where T_{bc} is the bulk temperature of the coolant, T_{max} is the maximum temperature of the wall, q'' is the heat flux per unit of surface uniformly imposed on the flat side of the finned plate [W/m^2], and k_c is the coolant coefficient of conductivity. They choose to represent effectiveness of the fin morphology by

$$E_c = \frac{q''}{q_r''} = \frac{h}{h_r} = \frac{h}{2.692K_c(\varsigma)^{1/3}/H}$$

where h_r is the global heat transfer coefficient of the **reference flat bottom plate** with the same hydraulic resistance ζ. They choose to define the **normalized** hydraulic resistance ς as:

$$\varsigma = \frac{(H^2)}{(12\mu\tilde{U}\langle m\rangle)}\left(-\frac{dp}{dx}\right)$$

Using the heterogeneous media simplified VAT\ performance characteristics for heat transfer in a flat channel with non specified morphologies of heat transfer enhancements results in the following:

a) heat transfer rate per unit volume per unit temperature difference

$$H_r = S_{all}\alpha_w^*/\Omega\ \left[\frac{W}{m^3 K}\right];$$

where S_{all} is the total internal surface, α_w^* is the combined (averaged over the all internal surfaces) heat transfer coefficient, and Ω is the volume of heat transfer; and

b) pumping power per unit volume P_p [W/m^3];

c) effectiveness parameter that results is

$E_{eff1} = H_r/P_p$

which will be discussed below.

II. EXPERIMENTAL SETUP

Wind tunnel

An open circuit suction-type wind tunnel was chosen to serve as a platform to study the heat transfer performance and pressure loss characteristics of augmented surfaces. The low-speed wind tunnel with an open circuit design is composed of the following sections: (a) an inlet section that includes flow conditioners like flow straighteners and turbulence control screens; (b) a contraction cone or nozzle that accelerates the flow; (c) test section that contains the model to investigate; (d) a diffuser that reduces the air speed with as little energy loss as possible; (e) a fan driven by a split capacitor motor that is controlled by an AC-V fan

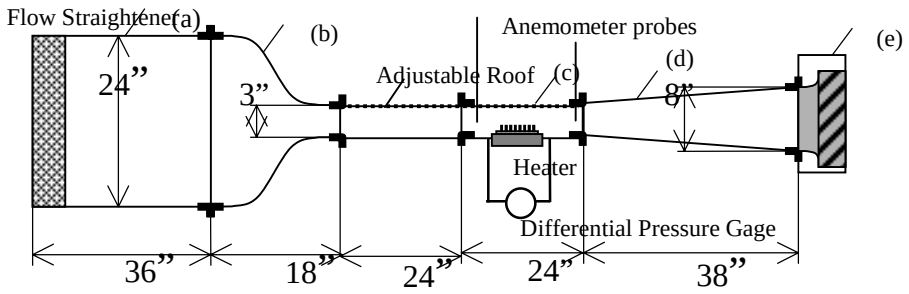

Figure 1 Overall view of the experimental rig and associated instrument.

speed control. The wind tunnel is operated in the suction mode; ie, the fan sucks atmospheric air through the fin assembly and the test section via the bell-mouthed entrance section, with the fan and motor assembly on the exhaust side of the system. This avoids the airstream being heated by the motor prior to its passage through the heat exchanger assembly. The body of the rectangular cross-sectioned wind-tunnel duct is made of Plexiglas. The duct is 4.5 inch wide and 1.5 inch high for the ‘no by-pass’ configuration. This material has been chosen because of the transparency and the low thermal conductivity, so that later use of a LDV system is allowed and heat losses from the wind tunnel are minimized. The roof of the long channel of the wind tunnel, over where the heat sink is located, is adjustable in height so that studies of the bypass effect can be done. The overall pressure drop through the heat sink is obtain via two static-pressure tapps located at the bottom of the test section. A standard differential pressure gage is used. In order to evaluate the velocity profile and the flow rate, velocity measurements were carried out using an air velocity transducer of cylindrical shape, which is inserted from the side walls of the test section. Measurements were taken upstream and downstream of the surface to be tested. A gutter of the same width as the transducer diameter is milled into the side walls of the channel to permit vertical movement of the transducer.

Heating system

A lot of effort has been put in the realization of a well calibrated heating system. The heat generating source plays an important role in the design of the experimental setup. It serves as a heat source in order to investigate the heat transfer to the environment and pressure loss characteristics of the augmented surface. Three cartridge heaters rated 250 W each were inserted into a copper block with the same area as the heat sinks (4.5” by 4.5”) and a thickness of 1 inch. Cartridge heaters have been put in parallel and wired to provide a maximum output power of 750 W. The emitted power (power = V×I) is controlled by a 120 V AC variac. Copper was for its high thermal conductivity (about 400 W/Km). The base assembly was firmly bolted together, as shown in Figure 2. The lower horizontal part and sides of the main heater copper block, such as sides of the heat sink were insulated thermally with 8 cm layer of fiber glass blanket, sandwiched with mica sheets.

A horizontal guard heater, rated at 160 W, was positioned parallel to the copper block, below one mica sheet and 2 cm of fiber glass, with the remaining 6 cm of insulating material placed below it. The whole system of heat generator, copper block and guard heater, with associated thermal insulation, was located in a well-fitting open-top wooden box. The power supplied to the cartridge heaters in the copper block could be adjusted by altering the variac setting and was measured by an in-line multimeter. The dissipation in the guard heater was adjusted until the steady state temperature difference across the mica sheet and the fiber glass, sandwiched between the two heaters, was zero. An estimation of the losses through the sides of the wooden box using thermocouples located on each side of the wooden box. The heat sink to be tested is mounted on the copper block. A thin layer of a high temperature resistant copper doped lubricant was applied at the interface between the heat sink and the copper block. The copper doped lubricant was chosen because of his lower viscosity compare with the standard thermal grease. The lower viscosity allows it to spread easily on the copper block surface achieving a very uniform thin layer. Furthermore, the copper lubricant can stand up to 2000 F when standard thermal grease or paste can stand only 400 F.

Under all the test conditions employed, more than 98% of the heat generated in the copper block passed, through the finned heat sink, to the air in the wind tunnel duct. The whole heater box is such that it can be taken apart and assembled easily in few minutes. Temperatures of the copper block were taken by an array of three K thermocouples; temperature profile of the heat sink base was provided by an array of three J thermocouples located along the air flow direction. To verify the quality of the model, temperatures along the pin fins are useful. For each of three pin fins of the heat sink along the flow direction, temperatures forward and backward were measured. Furthermore, the same pin fins were drilled to allow the collocation of two wires in order to measure the pin fin temperature at 1/3 and 2/3 of its height. Three narrow channels were grooved at the bottom of the aluminum heat sinks in order to guide the thermocouples out of the heat sink without affecting the surface contact between the aluminum heat sink and the copper block. The narrow channel, where the thermocouple wires were inserted, were then filled with high-conductivity thermal paste. This solution does not affect the air flow pattern into the heat sink. J thermocouples of 0.005” in diameter were used. The inlet and the oulet airstream temperatures in the wind tunnel duct were measured using a thermocouple located at the tip of the anemometer probe. Mapping the velocity profile a map of the temperature distribution is also done. Every thermocouple was calibrated before being installed.

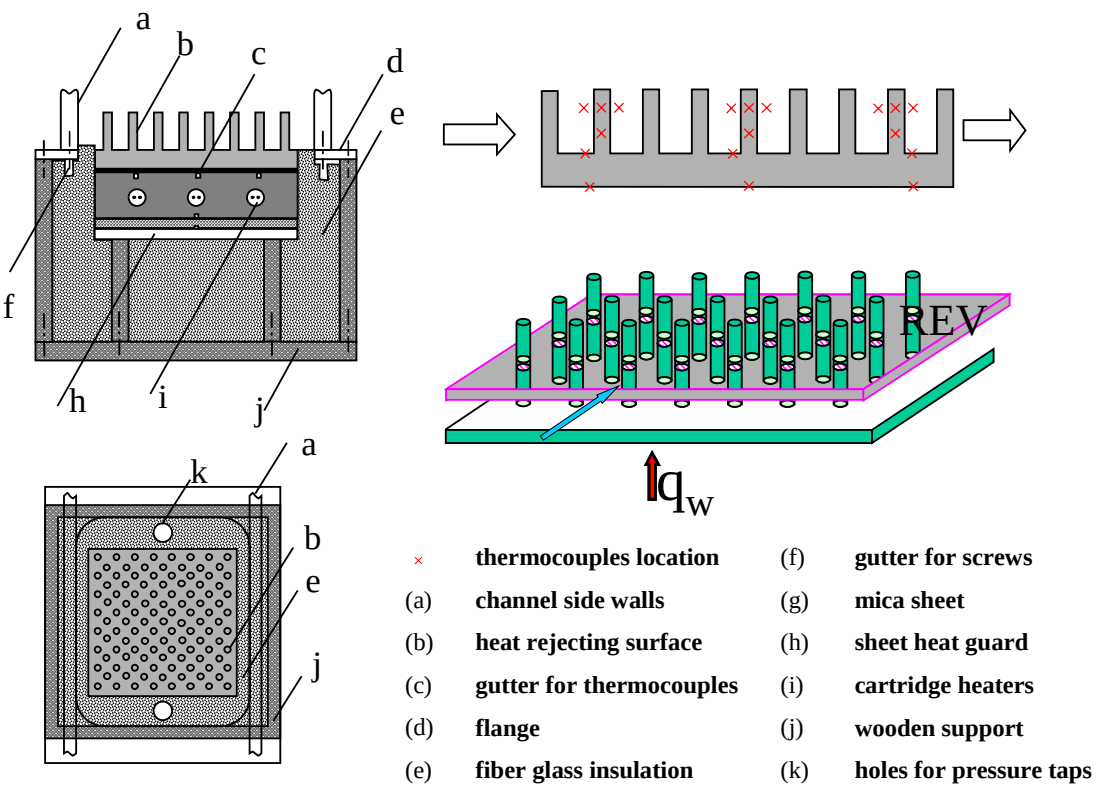

× **thermocouples location**

(a) **channel side walls**
(b) **heat rejecting surface**
(c) **gutter for thermocouples**
(d) **flange**
(e) **fiber glass insulation**
(f) **gutter for screws**
(g) **mica sheet**
(h) **sheet heat guard**
(i) **cartridge heaters**
(j) **wooden support**
(k) **holes for pressure taps**

Figure 2 View of the heat sink test fixture.

Heat Sink

The heat rejecting surface is of square shape with length of 11.43 cm (4.5 inch) and is made of aluminum with a conductivity of 225 W/m K. The construction method was to press fit round aluminum rods into a pre-drilled baseplate of thickness 0.25 inch (0.006m). Each of the three heat sinks had constant fin height (1.5 inch = 0.0381m), constant fin diameter (0.125 inch = 0.0381m), but the pitch was varied. All the three heat sinks tested had a *staggered* pin fin layout. The three interstitial (distance from pin center to pin center measured diagonally) pitches used were: P/d = 3/1, 9/4, 3/2. In order to ensure a tight fit between the pin fins and the base plate and to keep thermal losses in the interface to a minimum, the diameter of the holes incorporating the pin fins was slightly smaller than the one of the pin fins. The base plate was heated in an oven to more than 200 Celsius while the pin fins were stored in a freezer. The thermal expansion of the base, and of the hole size, and the thermal contraction of the pin fins, help to obtain a very tight interference fit between the two parts. Nevertheless, this procedure is non-optimal in terms of heat conduction from the base plate to the pin fins. This technique is considered to be sufficient for starting study simple morphology such as the staggered pin fins is. Future augmented surfaces will be monolithic.

Measurement uncertainties

In the present investigation, extra care was taken in constructing the heat transfer rig as well as in measuring the temperatures and the electrical power supplied. Each of the stated dimension was accurate to ± 0.2 mm, and the measured temperatures to ± 0.2 °C; whereas the differential pressure gage employed to measure the pressure drop was accurate to ± 0.05 inch of water (±12.4 Pa); the digital multimeter has an accuracy of ±1% rdg +4dgt for the AC Volts and ±2% rdg + 4dgt for the AC Current. The accuracy of the anemometer is ±0.02 m/s.

Experimental Procedure

The series of experiments were initiated with the fin array **#1,** corresponding to a P/d = 3. The heat sink was tested with NO-BYPASS for an input power of 50 W. the fan was set to reach the maximum velocity achievable. At steady state conditions, pressure drop and temperature were recorded. For the same input power, four different velocities were tested. Every time the steady state was assured before data was collected. The procedure was then repeated for input powers of 125 and 222 W. For every heat sink 12 data points have been taken. The different parameters and their values studied in this investigation are given in Table 1. The repeatability of the experiment was demonstrated by repeat testing.

Table 1 Parameter and their values

PARAMETER	VALUE
Diameter pin fin	0.3175 cm
Height pin fin	3.81 cm
Pitch h.s. staggered array **#1**	0.9525 cm
Pitch h.s. staggered array **#2**	0.71425 cm
Pitch h.s. staggered array **#3**	0.47625 cm
Heat input, Q_{in}	50,125,222W
By-pass	No
Re_{pore}	500 ÷ 20000

III. RESULTS AND DISCUSSION

The bulk (mean) Fanning friction factor f_f for the volume of the heat sink was assessed using formulae based on VAT for experimental measurements of pressure loss (see Travkin and Catton, 1998; Travkin et al., 1999):

$$f_f = \left[\frac{2\langle m \rangle \Delta p}{\rho_f \tilde{\tilde{U}}^2 S_w L_x} \right],$$

where $\tilde{\tilde{U}}$ is the average interstitial bulk velocity estimated for the volume where heat transfer occurs. The three samples studied show a consistent pattern of declining friction factor f_f with increasing porous media Reynolds number Re_{pore}, see Fig. 3. Some of the observed wavy like fluctuations of f_f were measured in other studies of cross-flow in tube bundles, see Zhukauskas chapter in Heat Exchangers Design Handbook (1983). The range of measured Fanning friction factor $0.45<f_f<0.8$ in Fig. 3 compares well with other well known correlations for Fanning friction factor in this range of Reynolds number defined using the VAT formulation (Travkin and Catton, 1998). The pumping power per unit volume for a heterogeneous media is given by the following:

$$P_p = \frac{P}{\Omega} = \frac{\dot{m} \Delta p}{\rho_f \Omega} = f_f \, \mathrm{Re}_{por}^3 \langle m_{yx} \rangle \left(\frac{S_w^4}{\langle m \rangle^4} \right) \frac{\mu^3}{128 \rho_f^2} \left[\frac{W}{m^3} \right],$$

where

$$\langle m_{yz} \rangle = \frac{S_{yz}}{L_y L_z}, \quad L_z = H,$$

and can be seen to be quite different from the expression usually used for a homogeneous media (Andrews and Fletcher, 1996):

$$P_{pm} = \frac{P}{\Omega} = f_f \, \mathrm{Re}_{por}^3 \wedge f_f^{1/3} \, \mathrm{Re}_{por} .$$

The factor $\langle m_{yx} \rangle \left(S_w^4 / \langle m \rangle^4 \right) \mu^3 / \left(128 \rho_f^2 \right)$ resulting from the VAT based treatment to obtain an expression for a heterogeneous media formula for pumping power can be associated with the morphological influence $\langle m_{yx} \rangle \left(S_w^4 / \langle m \rangle^4 \right)$ and with the physical characteristics of the cooling fluid $\mu^3 / \left(128 \rho_f^2 \right)$. The three samples of sink are depicted in Fig. 4. P_p was measured for a very broad range of Reynolds number $400<Re_{pore}<17000$.

A second, but more important characteristic to evaluate the heat exchange device, is the heat transfer rate $H_r = \left(S_{all} \alpha_w^* \right) / \Omega$ (see Fig. 5) for a known heat flux q_w through the bottom surface of heterogeneous volumetric devices used as heat exchangers from which the Nusselt number can be found:

$$H_r = \frac{S_{all} \alpha_w^*}{\Omega} = Nu_w \frac{k_f S_w}{4 \langle m \rangle} S_w^*, \left[\frac{W}{m^3 K} \right].$$

The Nu_w here is not an internal porous medium heat transfer Nusselt number. It is the bottom wall Nusselt number averaged across both phases. Implicitly it is - the overall (bottom and internal surface) Nusselt number including conjugate effects:

$$Nu_w = \frac{q_w d_{por}}{\left(T_{w\max} - T_{in} \right) k_f}$$

The conjugate effects are why it is so high for $80<Re_{pore}<800$ in the work by You and Chang (1997), who developed the same idea with only the temperature difference being used being different. They used averaged temperatures for both the bottom surface and internal air temperature.

Travkin and Catton (1998) and Travkin et al. (1999) recalculated a number of results found in the literature using the VAT based formulae, see Fig. 6, and found substantial differenced for this kind of combined heat transfer in comparison to internal media heat transfer coefficient correlations.

The ultimate parameter for most kinds of heat exchangers is the ratio of energy transfer rate to pumping power, H_r / P_p, which is the effectiveness of heat transfer per unit volume per unit temperature difference. For a heterogeneous volumetric two scale heat transfer device it is:

$$E_{eff1} = \frac{H_r}{P_p} = \left[\frac{Nu_w}{f_f \, \mathrm{Re}_{por}^3} \left(32 \frac{S_w^*}{\langle m_{yz} \rangle} \frac{\langle m \rangle^3}{S_w^3} \right) \frac{k_f \rho_f^2}{\mu^3} \right], \left[\frac{1}{K} \right],$$

which is distinguished from other expressions for effectiveness by the factor:

$$\left(32 \frac{S_w^*}{\langle m_{yx} \rangle} \frac{\langle m \rangle^3}{S_w^3} \right) \left(\frac{k_f \rho_f^2}{\mu^3} \right)$$

The effectiveness number E_{eff1} has been explicitly used for comparison of our three sink samples. Among parameters in the E_{eff1} expression, $S_w^* \left[1/m \right]$ is the overall specific surface in the volume of heat exchange - including internal surface area, S_{int}, and bottom wetted surface area, S_{wb}.

Also, the heat transfer rate, H_r (Fig. 5) and the Nusselt number (Fig. 6) curves, for all experiments (3×12=36), are different and dependent on the bottom the heat flux q_w. This is most likely a result of property dependence on temperature. How strong this effect appears depends on how the result is formulated. A great deal of effort was expended to assure ourselves that what was measured was real. Thus, this result does not confirm the assertion by You and Chang (1997) of heat flux independence. Further attention will be given to this result before a strong conclusion will be derived.

Fig. 7 presents measurements of the effectiveness based on the heterogeneous formulation of E_{eff1} and Fig 8 shows its counterpart based on the homogenous formulation. The conclusion drawn from these figures is that the three investigated versions of the same morphology have differing effectiveness in different ranges of momentum intensity (Re_{por}). The primary difference between the two figures is scale. The effectiveness defined using the VAT formulation, however, is much richer in that it contains the parameter dependence of lower scale on upper scale which the homogeneous formulation cannot.

IV. CONCLUSIONS

By comparing the three samples of round pin fin morphology of a semiconductor heat sink it is possible to make preliminary observations based on Figs. 3 and 5 that the third sample with the more dense packing of fins is the most effective among all three. This conclusion cannot be reached based on the homogeneous parameter based characteristics shown in Figs. 6 and 8 because they contradict one another. Fig. 6 suggests that the best among three samples is sample #1. Meanwhile, comparing effectivenesses in Fig. 8, indicates that the most effective configuration is sample #3. In our application the most important factor is how much energy can be transported outside of the heat sink, not the amount of energy used for this. Based on this reasoning, a designer can be compromised in favor of heat

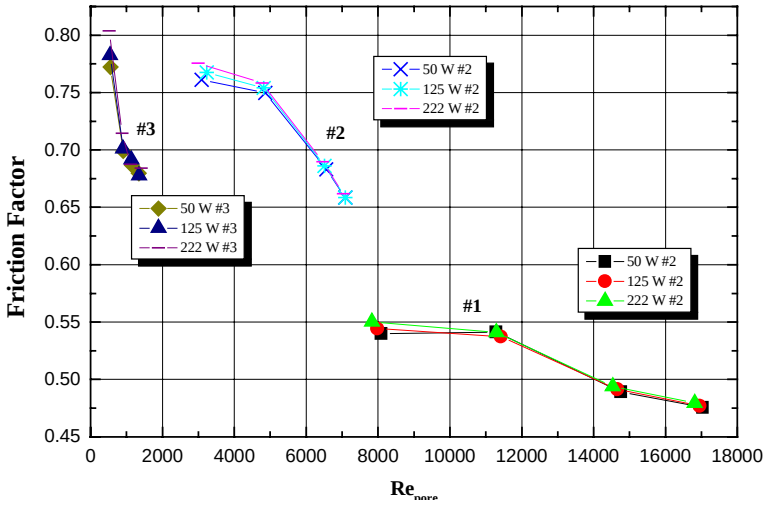

Figure 3

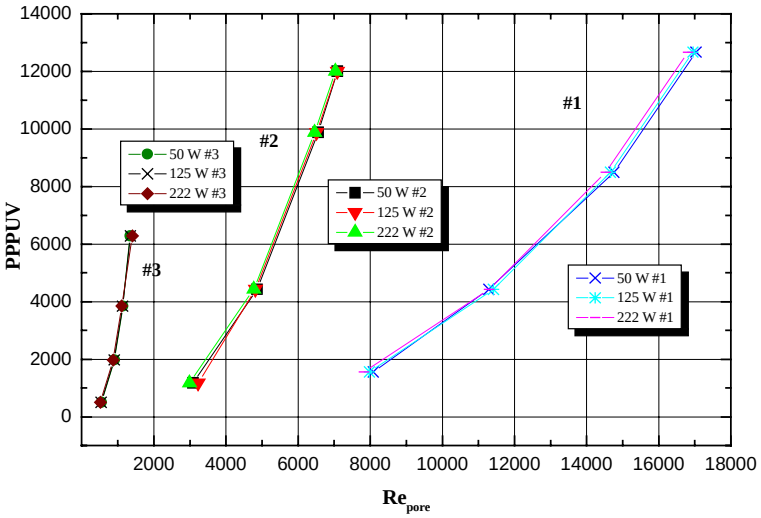

Figure 4

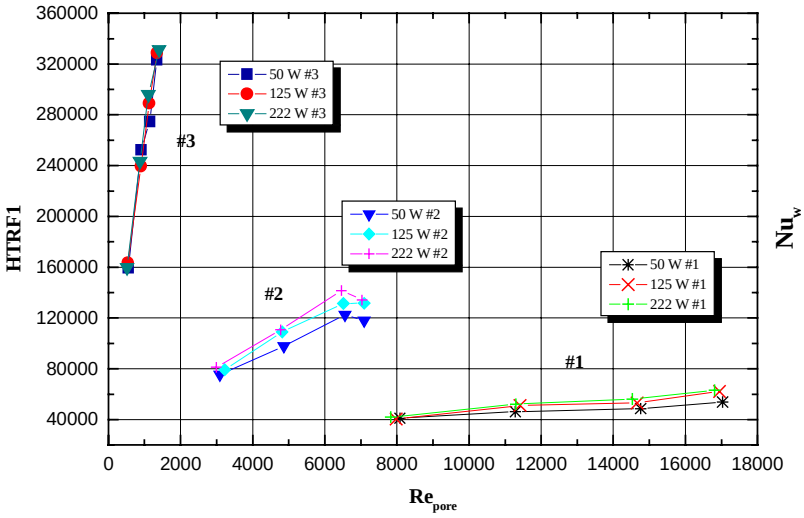

Figure 5

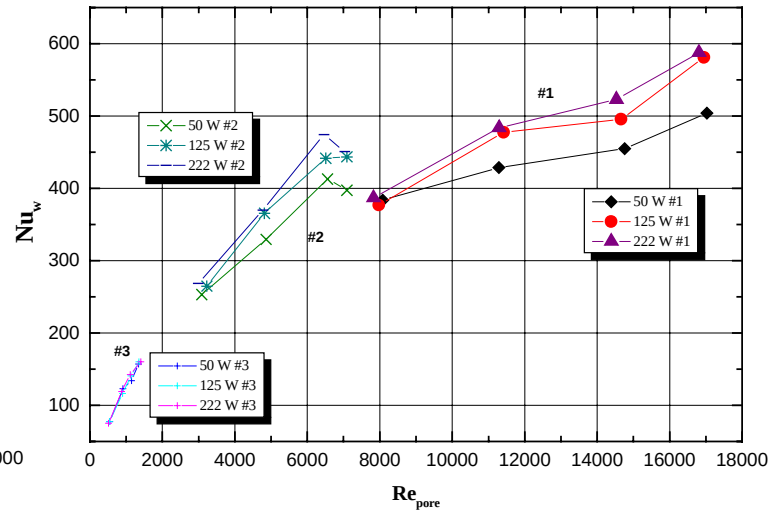

Figure 6

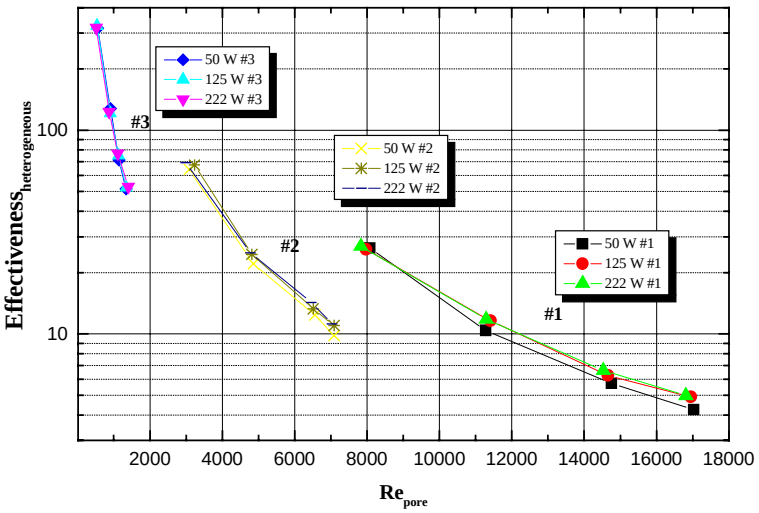

Figure 7

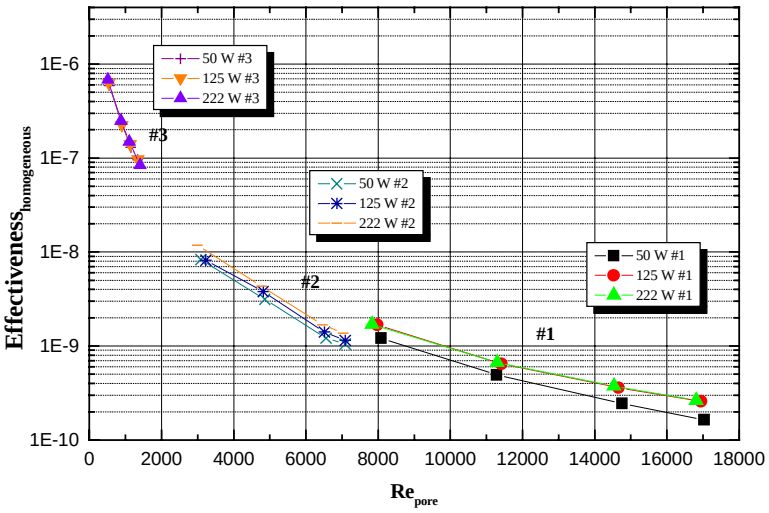

Figure 8

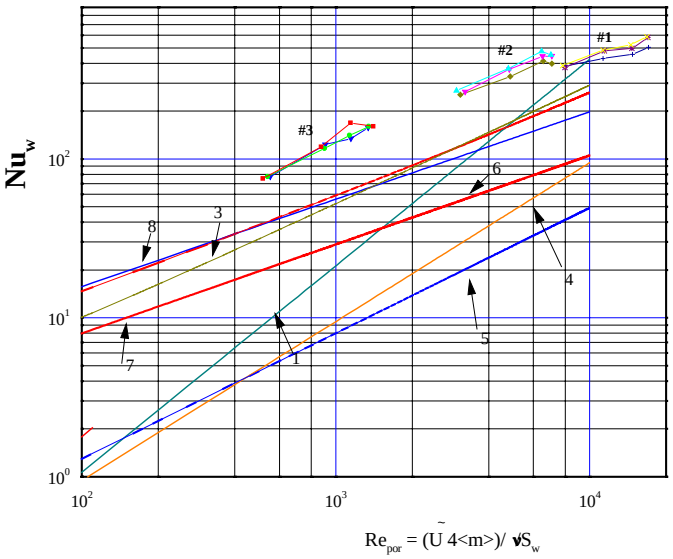

Figure 9 Internal effective heat transfer coefficient in porous media, reduced based on VAT scale transformations in experiments by: 3) Achenbach (1995); 5) Galitseysky and Moshaev (1993); 6) Kokorev et al. (1987); 7) Gortyshov (1987); 8) Kays and London (1984); **#1**, **#2**, **#3** experimental data.

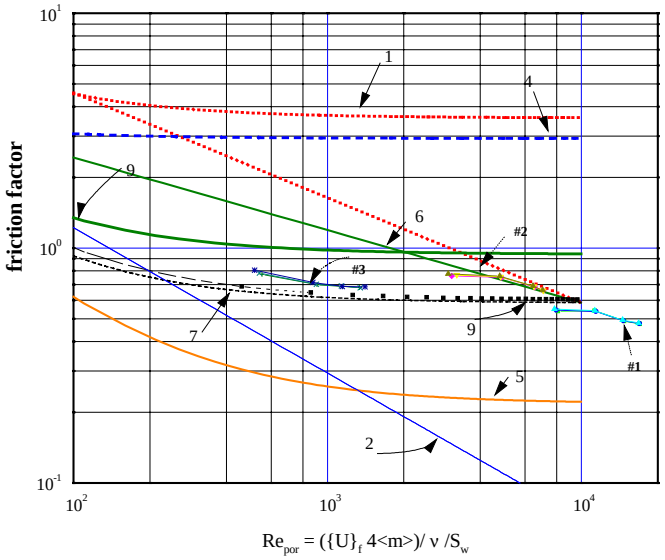

Figure 10 Fanning friction factor f\-(f) (bulk flow resistance in SVAT for different media morphologies, materials and scales used), reduced based on VAT scale transformations in experiments by: 1) Gortyshov et al. (1987); 2) Kays and London (1984); 4) Gortyshov et al. (1991); 5) Beavers and Sparrow (1969); 6) SiC foam (Travkin and Catton, 1997); 7) Ergun (1952); 9) Macdonald et al. (1979); **#1,#2,#3** experimental data.

sink #1, which is the least effective, but can withdraw the largest amount of heat in accordance with Nu_w in Fig. 6.

Further, the homogeneous effectiveness curves presented in Fig. 6 appear to show a continuous variation from high to low Reynolds numbers and that the data could be represented by a single curve. This could lead to an inappropriate conclusion about what heat sink configuration to use for a particular application. On the other hand, the heterogeneous representation clearly shows that there are other factors at play and that heat sink #1 may maintain its superiority over heat sink #2 at least for some ranges of Re_{pore}. It is clear that a broader range of Reynolds number needs to be investigated for each of the heat sinks and tha one needs to be careful in how conclusions are reached when the usual homogeneous parameter representation is used. The missing parameters relate the upper scale performance to the lower scale parameters and this is where optimization will take place. In spite a good coordination with the data of other experiments in Fig. 9,10 we would like to point out that as it appears the data reduction using simplified criteria as Re_{por}, f_f and Nu_w give a little or even wrong of desired information. We would present our findings related to data reduction criteria in following publication.

ACKNOWLEDGEMENTS

The authors would like to acknowledge the support of the Defense Advanced Research Projects Agency/Microsystems Technology Office project HERETIC and the Department of Energy, Office of Basic Energy Sciences through the grant DE-FG03-89ER14033 A002

REFERENCES

Andrews, M.J. and Fletcher, L.S., (1996), "Comparison of Several Heat Transfer Enhancement Technologies for Gas Heat Exchangers," *J. Heat Transfer*, Vol. 118, pp. 897-902.

Bejan, A. and Morega, A.M., (1993), "Optimal Arrays of Pin Fins and Plate Fins in Laminar Forced Convection," *Journal of Heat Transfer*, Vol. 115, pp. 75-81.

Bejan, A. (1995), "The Optimal Spacing for Cylinders in Crossflow Forced Convection," *Journal of Heat Transfer*, Vol. 117, pp. 767-770.

Fabbri, G., (1999), "Optimum Performances of Longitudinal Convective Fins with Symmetrical and Asymmetrical Profiles", *Int. J. Heat Fluid Flow*, Vol. 20, pp. 634-641.

Jubran, B.A., Hamdan, M.A., and Abdualh, R.M. (1993), "Enhanced Heat Transfer, Missing Pin, and Optimization for Cylindrical Pin Fin Arrays," *J. Heat Transfer*, Vol. 115, pp. 576-583.

Kim, S.J. and D.Kim, (1999), "Forced Convection in Microstructures for Electronic Equipment Cooling," *J. Heat Transfer*, Vol. 121, No.3, pp. 639-645.

You, H.-I.,and Chang, C.-H. (1997), "Numerical Prediction of Heat Transfer Coefficient for a Pin-Fin Channel FLow", *Journal Heat Tansfer*, Vol. 119, No. 4, pp. 840 843.

Heat Exchanger Design Handbook, 1983, (Spalding, B.D., Taborek, J., Armstrong, R.C. and et al., contribs.), N.Y., Hemisphere Publishing Corporation, Vol.1,2.

Gratton, L., Travkin, V.S., and Catton, I., (1996), "The Influence of Morphology upon Two- Temperature Statements for Convective Transport in Porous Media," *Journal of Enhanced Heat Transfer*, Vol. 3, No. 2, pp.129-145.

Travkin V. S. and Catton, I., 1998, A two temperature model for turbulent flow and heat transfer in a porous layer, *Advances in Colloid and Interface Science*, Vol. 76-77, pp. 389-443.

V.S. Travkin, I. Catton, K. Hu, A.T. Ponomarenko, and V.G. Shevchenko, (1999), "Transport Phenomena in Heterogeneous Media: Experimental Data Reduction and Analysis", in *Proc. ASME, AMD-233*, Vol. 233, pp. 21-31.

Travkin, V.S., Catton, I., and Hu, K., (2000), "Optimization of Heat Transfer Effectiveness in Heterogeneous Media," in *print in Proceedings of the Eighteenth Symposium on Energy Engineering Sciences*, Argonne National Laboratory.